Available online at www.sciencedirect.com
ScienceDirect
Journal of Power Sources 159 (2006) 1300–1304
JOURNAL OF POWER SOURCES
www.elsevier.com/locate/jpowsour

Short communication

A composite visible-light photocatalyst for hydrogen production

Yiliang Liu [a], Liejin Guo [a,*], Wei Yan [a], Hongtan Liu [a,b]

[a] *State Key Laboratory of Multiphase Flow in Power Engineering (SKLMF), Xi'an Jiaotong University, Xi'an 710049, PR China*
[b] *Dorgan Solar Energy and Fuel Cell Laboratory, Department of Mechanical and Aerospace Engineering, University of Miami, FL, USA*

Received 26 September 2005; accepted 17 November 2005
Available online 23 February 2006

Abstract

A composite photocatalyst, Pd–$TiO_{2-x}N_x$–WO_3, was synthesized by the template method and characterized by energy dispersive X-ray microanalysis (EDX), X-ray diffraction (XRD), UV–vis spectrometer, and scanning electron microscope (SEM). The results of EDX analysis reveals that the molecular formula of the composite photocatalyst can be expressed as Pd–$TiO_{1.72}N_{0.28}$–WO_3. The UV–vis absorption spectrum indicates that the absorption edge of the catalyst red-shifts to around 600 nm. Under the irradiation with ultraviolet and visible light, the catalyst showed good performance for photocatalytic hydrogen production with a Na_2S/Na_2SO_3 system as the sacrificial agent.

Keywords: Photocatalyst; TiO_2; Hydrogen; Visible light

1. Introduction

Since photoinduced decomposition of water on TiO_2 electrode was discovered, semiconductor photocatalysts have attracted much interest. However, to date, most photocatalysts are capable of absorbing only ultraviolet light, which accounts for only about 4% of incoming solar energy. Therefore, recent research has been focused on developing photocatalysts that are capable of utilizing the less energetic visible light, which accounts for about 43% of incoming solar energy.

In recent years, the search for visible-light photocatalysts has made considerable progress. Asahi et al. [1] developed a new photocatalyst $TiO_{2-x}N_x$ by doping TiO_2 with nitrogen. They demonstrated that the new photocatalyst had an improvement over TiO_2 both in optical absorption and photocatalytic activity under visible light. Heyduk and Nocera [2] reported the use of a two-electron mixed-valance dirhodium compound to photocatalyze the reduction of hydrohalic acid to hydrogen under visible light. Zou et al. [3] developed a series of photocatalysts of indium–tantalum-oxide doped with nickel, $In_{1-x}Ni_xTaO_4$ ($x = 0$–0.2), which could induce direct splitting of water into stoichiometric amounts of oxygen and hydrogen under visible-light irradiation. Shahed et al. [4] synthesized a carbon-doped n-type TiO_2 photocatalyst, n-$TiO_{2-x}C_x$, which could absorb light at wavelengths below 535 nm and split water to hydrogen under illumination with visible light. Bessekhouad et al. [5] showed that $CuMnO_2$ had the ability for photocatalytic hydrogen production from water under visible-light illumination. Recently, Kudo et al. [6–8] developed a series of band-structure-controlled photocatalysts, $(AgIn)_xZn_{2(1-x)}S_2$, $(CuIn)_xZn_{2(1-x)}S_2$, and ZnS–$CuInS_2$–$AgInS_2$, which all had comparatively high activity to produce hydrogen from water under visible irradiation.

It is well known that two of the key issues in photocatalyst research are to make semiconductors absorb visible light and to hinder photogenerated electrons-hole recombinations. Using a narrow band-gap semiconductor to combine with TiO_2 can broaden its photoresponsive range under visible light, such as TiO_2–WO_3 [9], CdS–TiO_2 [10], etc. Furthermore, loading noble metals onto the photocatalyst mainbody can separate photogenerated electrons and holes more effectively and thus improve the hydrogen evolution efficiency, such as Pt–TiO_2 [11,12] or Au–TiO_2 [12].

In this work, a novel semiconductor composite photocatalyst, Pd–$TiO_{2-x}N_x$–WO_3, was designed. The catalyst was prepared by the sol–gel method with an inorganic palladium salt, $Pd(NH_3)_2Cl_2$, as the structure-directing agent [13]. Its performance in photocatalytic hydrogen production from water under ultraviolet and visible light was studied.

* Corresponding author. Tel.: +86 29 82663895; fax: +86 29 82669033.
E-mail address: lj-guo@mail.xjtu.edu.cn (L. Guo).

0378-7753/$ – see front matter © 2006 Elsevier B.V. All rights reserved.
doi:10.1016/j.jpowsour.2005.11.105

2. Experimental

2.1. Preparation and characterization of photocatalyst

All chemical reagents were commercially purchased and used without further treatments.

2×10^{-4} mol $Pd(NH_3)_2Cl_2$ (Shanghai Chem. Co. I, >99%) was dispersed in 25 mL deionized water using an ultrasonic oscillator, and then 250 mL ethanol (Xi'an Chem. Co., >99.5%) was added to the blend. After the above mixture was cooled to −70 °C by liquid nitrogen while stirring [13], 17 mL tetrabutylorthotitanate (Beijing Zhonglian Chem. Co., >98.5%) was added to the mixture drop by drop. Then, 0.4 mol L^{-1} ammonia solution was dropwise added into the mixture until the pH value reached 7.0. After 12 h when about all the titanate species had hydrolyzed into TiO_2 colloids, the liquid nitrogen was removed and the temperature of the mixture was allowed to slowly increase to room temperature. Then the obtained product was filtered to obtain a gel, which was re-dispersed in deionized water using an ultrasonic oscillator. After adding 200 mL 0.1 mol L^{-1} ammonium tungstate (Shanghai Chem. Co. II, >99%) aqueous solution, the dispersed mixture was dried at 70 °C. The solid mixture was calcined for 2 h at 600 °C and a yellowish powder was obtained.

In addition, the pure TiO_2 used as the reference photocatalyst was synthesized from tetrabutylorthotitanate as the titanium source, using the same process as described above. $TiO_{2-x}N_x$ was prepared by mixing 2.0 g TiO_2 gel obtained above with 1.68 g $(NH_4)_2CO_3$ (Xi'an Chem. Co., >99%) and calcining the solid mixture for 4 h at 400 °C under N_2 atmosphere. During this process, $(NH_4)_2CO_3$ was decomposed into NH_3, CO_2 and H_2O. At the same time, the nitrogen atoms in NH_3 substituted some oxygen atoms in TiO_2, forming $TiO_{2-x}N_x$ [14,15].

Element analysis was carried out on EDAX DX-4 (Philips Co.), and SEM images were obtained from a Hitachi-530 scanning electron microscope. The crystal structure of the sample was identified by XRD (Type Shimadzu Rax-10) with graphite monochromized Cu Kα radiation (45 kV, 15 mA). UV–vis spectrum was obtained with HITACHI340 UV–vis spectrometer.

2.2. Photocatalytic reaction

The photocatalytic reaction was carried out in an inner-irradiation type reactor. The photocatalyst powder (50 mg) was dispersed by a magnetic stirrer in 150 mL aqueous solution containing 0.1 mol L^{-1} Na_2S and 0.04 mol L^{-1} Na_2SO_3 as the sacrificial agents. A 300 W high-pressure mercury lamp (Changzhou Yuyu Co., UV-300) was used as the light source. Before the irradiation, the reactor was purged with nitrogen for about 30 min to remove air. The gas evolved was gathered by drainage and it was analyzed by GC–MS using a C18 column and nitrogen as the carrier gas. During the entire experiment, the reaction temperature was kept at 25 ± 0.2 °C.

In the experiment under visible light, 1 mol L^{-1} $NaNO_2$ solution was introduced as the internal circulation condensate agent to remove light with wavelengths shorter than 400 nm. The UV–vis spectrum of the $NaNO_2$ solution showed that it could effectively absorb light with wavelengths below 400 nm and thus act as a cutoff filter.

The light intensity of the high-pressure mercury lamp was measured using $KFe(C_2O_4)_2$ as the chemical actinometer [16]. The number of incident photons during the photocatalytic reaction was determined with the following equation:

$$\text{Number of incident photons} = \text{light intensity} \times \text{irradiated area} \times \text{reaction time} \quad (1)$$

The apparent quantum efficiency was determined with the following equation [6]:

$$\text{AQE}(\%) = \frac{\text{number of reacted electrons}}{\text{number of incident photons}} \times 100\% = \frac{\text{number of evolved } H_2 \text{ molecules} \times 2}{\text{number of incident photons}} \times 100\% \quad (2)$$

In addition, the apparent energy conversion efficiency was determined with the following equation [17]:

$$\text{AECE}(\%) = \frac{\text{combustion enthalpy of evolved } H_2}{\text{energy of incident photons}} \times 100\% \quad (3)$$

3. Results and discussion

3.1. Characterization

Element analysis of the catalyst indicates that the content of palladium is 1.45 wt.% and that of tungsten is 43.59 wt.%. The molecular ratio of Ti to N is 1:0.28, and thus the composite catalyst can be expressed as $Pd–TiO_{1.72}N_{0.28}–WO_3$.

Fig. 1 shows the XRD pattern of $Pd–TiO_{1.72}N_{0.28}–WO_3$. From this figure we can see that, the highest peak of the composite catalyst is at $2\theta = 25.2°$, almost the same as that of pure TiO_2 and $TiO_{2-x}N_x$, indicating that the crystal structure of $TiO_{1.72}N_{0.28}$ in the composite catalyst is principally anatase [18]. In plot 3, the peak at $2\theta = 23.6°$ is the characteristic peak of WO_3 monoclinic phase [19], which confirms the existence

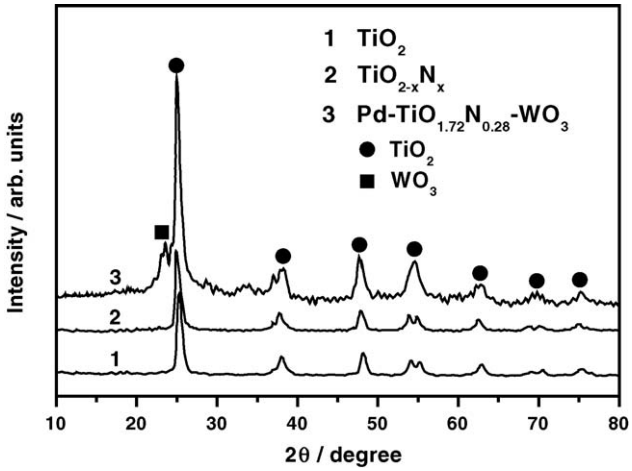

Fig. 1. XRD pattern of $Pd–TiO_{1.72}N_{0.28}–WO_3$.

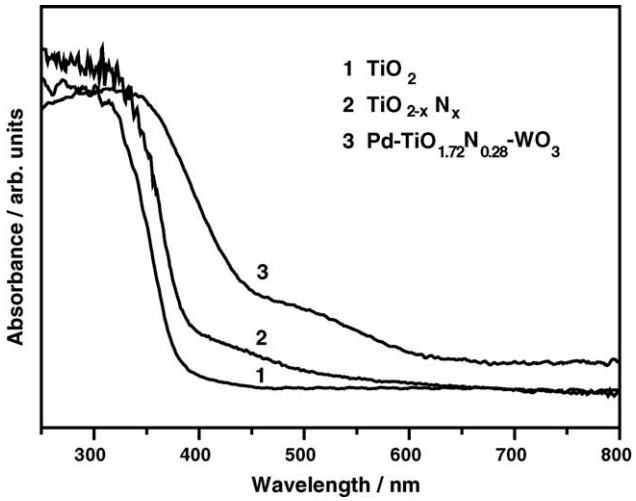

Fig. 2. UV–vis spectrum of Pd–$TiO_{1.72}N_{0.28}$–WO_3.

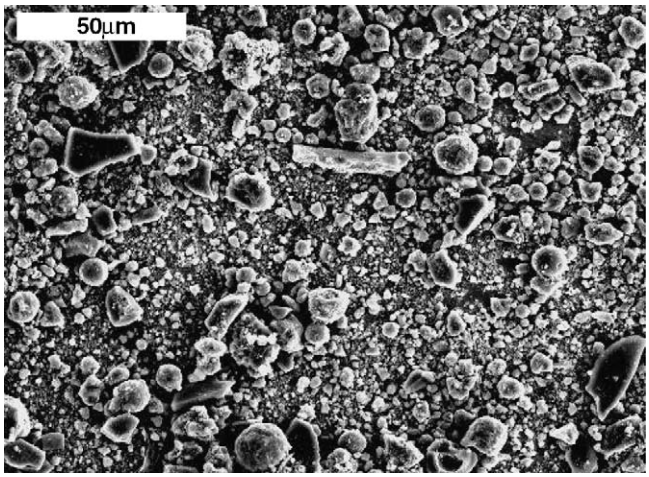

Fig. 3. SEM image of Pd–$TiO_{1.72}N_{0.28}$–WO_3.

of WO_3 crystals and its crystal structure. The average particle sizes of Pd–$TiO_{1.72}N_{0.28}$–WO_3, pure TiO_2 and $TiO_{2-x}N_x$ are determined to be 10.73, 10.96 and 10.60 nm, respectively, by the Scherrer formula. In addition, the surface areas of these three photocatalysts are found to be 68.8, 64.0, and 69.1 $m^2\ g^{-1}$, respectively, using the Brunauer–Emmett–Teller (BET) method.

Fig. 2 shows the UV–vis spectrum of Pd–$TiO_{1.72}N_{0.28}$–WO_3, indicating that the absorption edge of the catalyst in visible-light region extends to about 600 nm, which is greater than that of TiO_2 (387.5 nm) [18], WO_3 (481 nm) [19], $TiO_{2-x}N_x$ (500 nm) [1] and $TiO_{2-x}C_x$(535 nm) [4]. The underling mechanism could be multifactor coupling. Firstly, in $TiO_{1.72}N_{0.28}$, the N p states can mix with O 2p states, and thus the dominant transitions at the absorption edge have been identified with those from N $2p_\pi$ to Ti d_{xy}, instead of from O $2p_\pi$ as in TiO_2 [1,20]. This change makes the maximum absorption wavelength of $TiO_{1.72}N_{0.28}$ red-shift [1]. Secondly, because the Ti 3d and the W 5d levels have nearly the same energy, Ti^{4+} and W^{6+} cations can strongly interact and mix with each other [9]. Thus, introducing WO_3 into TiO_2 results in the absorbance of light with longer wavelength [18]. In summary, it is the interaction of these two factors that makes the absorption wavelength of the synthesized catalyst red-shift to around 600 nm.

Fig. 3 shows the SEM image of Pd–$TiO_{1.72}N_{0.28}$–WO_3, from which we can see that the catalyst particles are spherical. When cubic $Pd(NH_3)_2Cl_2$ polycrystals are used as the templates, TiO_2 colloids wrap around them and form the spherical shapes.

The formation mechanism of this composite catalyst could be explained as below. During the process of synthesis, the insoluble $Pd(NH_3)_2Cl_2$ may serve as the template after being dispersed in water. At a low temperature of −70 °C, tetrabutylorthotitanate reacts very slowly. As a result, it can hydrolyze more thoroughly and produce smaller colloid particles. At the same time, the intermediate titanate species can interact with the NH_3 ligands of the template molecules at the surface of the crystals via hydrogen bonds [13]. Then TiO_2 colloids grow at the surface of the template crystals through condensation processes and enclose them. After adding the ammonium tungstate aqueous solution to the colloids, the ammonium tungstate molecules diffuse into the TiO_2 colloids as well as attach to their surfaces. In the process of calcining the colloids mixture at 600 °C, the template molecules decompose into metallic palladium particles, which are wrapped inside by TiO_2 colloids; while the ammonium tungstate decomposes into WO_3 particles, which attach to the outside of TiO_2 colloids. At the same time, the nitrogen atoms in ammonium ions are doped into TiO_2, forming $TiO_{2-x}N_x$.

3.2. Photocatalytic activity

Fig. 4 shows the hydrogen production performances of Pd–$TiO_{1.72}N_{0.28}$–WO_3, pure TiO_2, and $TiO_{2-x}N_x$ under ultraviolet light. From this figure we can see that, after 180 min irradiation, the amount of hydrogen production on Pd–$TiO_{1.72}N_{0.28}$–WO_3 is 4045 μmol, which is significantly greater than 2232 and 1775 μmol, the respective amounts of hydrogen production on pure TiO_2 and $TiO_{2-x}N_x$. In addition, the rate of hydrogen evolution on Pd–$TiO_{1.72}N_{0.28}$–WO_3 is steady, indicating that the catalyst has good and stable photo-

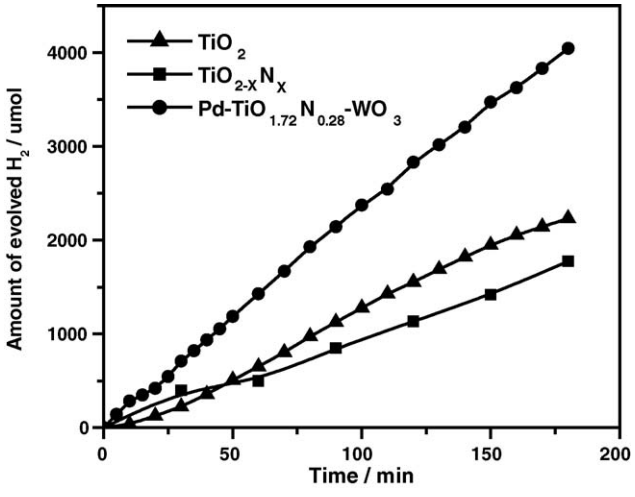

Fig. 4. Hydrogen production performances of TiO_2, $TiO_{2-x}N_x$, and Pd–$TiO_{1.72}N_{0.28}$–WO_3 under ultraviolet light.

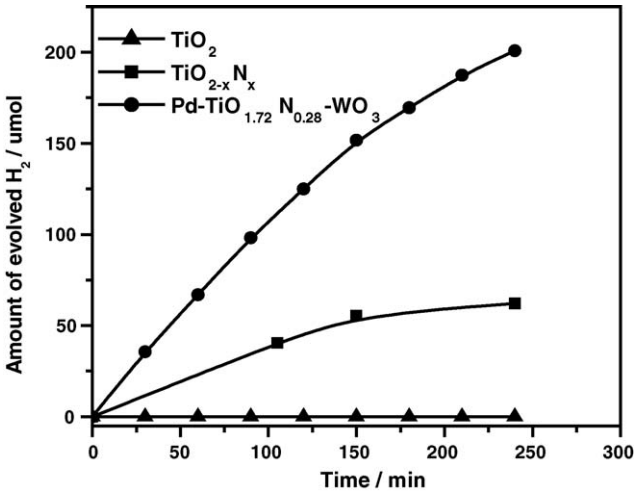

Fig. 5. Hydrogen production performances of TiO_2, $TiO_{2-x}N_x$, and Pd–$TiO_{1.72}N_{0.28}$–WO_3 under visible light.

catalytic activity under ultraviolet light irradiation. The apparent quantum efficiencies of Pd–$TiO_{1.72}N_{0.28}$–WO_3, pure TiO_2, and $TiO_{2-x}N_x$ under ultraviolet light are determined to be 3.40%, 1.88% and 1.49%, respectively, from Eq. (2). Their apparent energy conversion efficiencies are found to be 1.44%, 0.79% and 0.63%, respectively, from Eq. (3).

Fig. 5 shows the hydrogen production performances of Pd–$TiO_{1.72}N_{0.28}$–WO_3, pure TiO_2, and $TiO_{2-x}N_x$ under visible-light irradiation. The amount of hydrogen production on Pd–$TiO_{1.72}N_{0.28}$–WO_3 is 201 μmol after 240 min irradiation, while that on $TiO_{2-x}N_x$ is 62 μmol, and that on TiO_2 is negligible. The apparent quantum efficiencies of Pd–$TiO_{1.72}N_{0.28}$–WO_3 and $TiO_{2-x}N_x$ under visible light are determined to be 0.45% and 0.14%, respectively, and their apparent energy conversion efficiencies are 0.23% and 0.07%, respectively.

Since it is impossible to determine the exact number of photons absorbed by the photocatalysts, the total incident light is employed in calculating the apparent quantum efficiencies and energy conversion efficiencies. In this case, the apparent efficiencies obtained from Eqs. (2) and (3) are lower than the actual efficiencies.

3.3. Mechanism of photocatalytic reaction

The energy band of TiO_2 is composed of a low-energy valence band full of electrons and a high-energy conduction band with no electron. When the energy absorbed by an electron is greater than the band-gap energy, the excited electron may transfer to the conduction band, leaving a positive hole in the valence band. Then, both the photogenerated electrons and holes may migrate to the surfaces of the catalyst particles and proceed with oxidation–reduction reactions, respectively, with the locally absorbed species.

In general, there are two factors affecting the activity of a photocatalyst under visible light. The first one is its absorption performance in visible-light region, and the second one is its separation efficiency of photogenerated electrons and holes. On one hand, as shown in Fig. 2, the light absorption of Pd–$TiO_{1.72}N_{0.28}$–WO_3 extends to around 600 nm, farther than that of pure TiO_2 and WO_3, indicating that the composite photocatalyst may utilize light more effectively.

On the other hand, the coexistence of Pd and WO_3 with TiO_2 may lower the recombination probability between photogenerated electrons and holes in the composite catalyst, and thus improve the efficiency of photocatalysis. It is well known that there are two forms of electron-hole recombination in TiO_2, surface recombination and bulk recombination, and both can lower the efficiency of photocatalysis. The Fermi energy level of Pd is lower than that of TiO_2, and since they are closer to each other, the electrons on the surface of TiO_2 can spontaneously transfer to the surface of Pd until their Fermi energy levels become equal. As a result, excessive negative charges accumulate on the surface of Pd and excessive positive charges accumulate on the surface of TiO_2. Therefore, the energy band of TiO_2 bends upwards, forming the Schottky barrier as shown in Fig. 6. In this sense, in the composite catalyst, Pd acts as an electron trap, which can effectively prevent the surface electron-hole recombination.

In addition, when irradiated by light with enough excitation energy, the band-to-band transition will occur simultaneously both in TiO_2 and WO_3. Because TiO_2 and WO_3 have different conduction band and valence band energy levels, some of the photogenerated electrons in the conduction band of TiO_2 may spontaneously transfer to the low-level conduction band of WO_3, and some of the photogenerated holes may accumulate in the high-level valence band of TiO_2, as shown in Fig. 7. As a result, the separation efficiency of photogenerated electron-hole couples in TiO_2–WO_3 could be higher than those in pure TiO2 and WO_3.

Because the conduction band potential of WO_3 is more positive than the potential of H^+/H_2, the accumulated electrons in its conduction band cannot reduce H^+ to H_2, and thus do not contribute to the photocatalytic efficiency. However, as Fig. 4

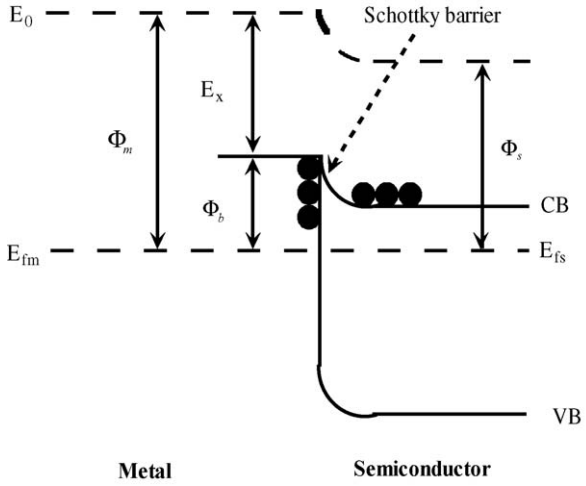

Fig. 6. Schottky barrier between a metal and a semiconductor. E_{fm}: Fermi energy level of the metal; E_{fs}: Fermi energy level of the semiconductor; E_0: energy of static electron in vacuum; Φ_m: work function of the metal; Φ_s: work function of the semiconductor; E_x: electron affinity energy; Φ_b: height of Schottky barrier.

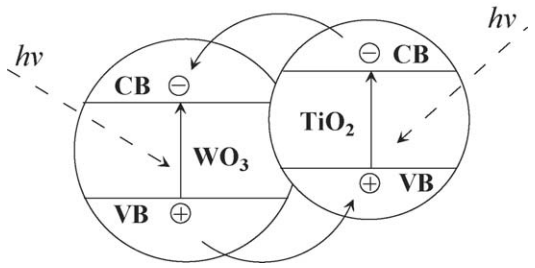

Fig. 7. Transference of charge carriers in TiO_2–WO_3 composite semiconductor.

shows, despite this disadvantage, the hydrogen evolution rate of Pd–$TiO_{1.72}N_{0.28}$–WO_3 is still higher than that of pure TiO_2, indicating that introducing Pd and WO_3 to TiO_2 indeed has certain advantages. This work provides a direction for future development of visible-light photocatalysts. Seeking a narrow band-gap semiconductor with conduction band potential more negative than the H^+/H_2 electrode potential to replace WO_3 in the composite catalyst, may achieve higher activity of hydrogen production.

Furthermore, another method for preventing photogenerated electrons from recombining with photogenerated holes is to scavenge the holes with sacrificial electron donors. Therefore, an electron donor system, Na_2S/Na_2SO_3, was employed in our work to scavenge the holes generated in the valance band of the composite photocatalyst. The S^{2-} could seize the holes effectively and produce ${S_2}^{2-}$, which was in turn renewed to S^{2-} by ${SO_3}^{2-}$, as shown in the equations below [21,22]:

$$2S^{2-} + 2h^+ \rightarrow {S_2}^{2-} \quad (4)$$

$${S_2}^{2-} + {SO_3}^{2-} \rightarrow S^{2-} + {S_2O_3}^{2-} \quad (5)$$

4. Conclusions

In order to improve both the absorption performance of photocatalysts in the visible-light region and the separation efficiency of photogenerated electrons and holes, a composite photocatalyst Pd–$TiO_{2-x}N_x$–WO_3 was synthesized by the template method using Pd, $TiO_{2-x}N_x$ and WO_3 as the three components. The results of element analysis indicate that the molecular formula of the composite catalyst can be expressed as Pd–$TiO_{1.72}N_{0.28}$–WO_3. The XRD pattern of the composite catalyst confirms the existence of $TiO_{1.72}N_{0.28}$ and WO_3, and their crystal structures (anatase and monoclinic phase, respectively). UV–vis spectrum indicates that this catalyst is capable of absorbing light with wavelengths up to 600 nm. During the photocatalytic reaction, the catalyst shows comparatively good activities for hydrogen production under both ultraviolet light and visible light. In addition, a possible mechanising is presented to explain the improved photocatalytic activity of this composite catalyst.

Acknowledgments

This work was supported by the National Natural Science Foundation of China (No. 90210027) and the National Basic Research Program of China (No.2003CB214500).

References

[1] R. Asahi, T. Morikawa, O.K. Aoki, Y. Taga, Science 293 (2001) 269–271.
[2] A.F. Heyduk, D.G. Nocera, Science 293 (2001) 1639–1641.
[3] Z.G. Zou, J.H. Ye, K. Sayama, H. Arakawa, Nature 414 (2001) 625–627.
[4] U.M. Khan Shahed, M. Al-Shahry, W.B. Ingler, Science 297 (2002) 2243–2245.
[5] Y. Bessekhouad, M. Trari, J.P. Doumerc, Int. J. Hydrogen Energy 28 (2003) 43–48.
[6] I. Tsuji, H. Kato, H. Kobayashi, A. Kudo, J. Am. Chem. Soc. 126 (2004) 13406–13413.
[7] I. Tsuji, H. Kato, H. Kobayashi, A. Kudo, J. Phys. Chem. B 109 (2005) 7323–7329.
[8] I. Tsuji, H. Kato, A. Kudo, Angew. Chem. Int. Ed. 44 (2005) 3565–3568.
[9] A.G. Alejandre, J. Ramirez, G. Busca, Langmuir 14 (1998) 630–639.
[10] H. Fujii, M. Ohtaki, K. Eguchi, H. Arai, J. Mol. Catal. A: Chem. 129 (1998) 61–68.
[11] U. Siemon, D. Bahnemann, J.J. Testa, D. Rodriguez, M.I. Litter, N. Bruno, J. Photochem. Photobiol. A: Chem. 148 (2002) 247–255.
[12] G.R. Bamwenda, S. Tsubota, T. Nakamura, M. Haruta, J. Photochem. Photobiol. A: Chem. 89 (1995) 177–189.
[13] C. Hippe, M. Wark, E. Lork, G.S. Ekloff, Micropor. Mesopor. Mater. 31 (1999) 235–239.
[14] S. Sakthivel, M. Janczarek, H. Kisch, J. Phys. Chem. B 108 (2004) 19384–19387.
[15] R. Nakamura, T. Tanaka, Y. Nakato, J. Phys. Chem. B 108 (2004) 10617–10620.
[16] G. Bi, S.Z. Tian, Z.G. Feng, J.K. Cheng, J. Anal. Sci. 11 (1995) 15–19.
[17] G.Q. Guan, T. Kida, K. Kusakabe, K. Kimura, X.M. Fang, T.L. Ma, E. Abe, A. Yoshida, Chem. Phys. Lett. 385 (2004) 319–322.
[18] X.Z. Li, F.B. Li, C.L. Yang, W.K. Ge, J. Photochem. Photobiol. A: Chem. 141 (2001) 209–214.
[19] G.R. Bamwenda, K. Sayama, H. Arakawa, J. Photochem. Photobiol. A: Chem. 122 (1999) 175–183.
[20] R. Aashi, Y. Taga, Phys. Rev. B 61 (2000) 7459–7465.
[21] N. Bühler, K. Meier, J.F. Reber, J. Phys. Chem. 88 (1984) 3261–3268.
[22] J.F. Reber, K. Meier, J. Phys. Chem. 88 (1984) 5903–5913.